International Journal of Pharmaceutics 422 (2012) 24–32

Contents lists available at SciVerse ScienceDirect

International Journal of Pharmaceutics

journal homepage: www.elsevier.com/locate/ijpharm

Characterisation, solubility and intrinsic dissolution behaviour of benzamide: dibenzyl sulfoxide cocrystal

Christine Grossjohann[a], Kevin S. Eccles[b], Anita R. Maguire[c], Simon E. Lawrence[b], Lidia Tajber[a], Owen I. Corrigan[a], Anne Marie Healy[a,*]

[a] School of Pharmacy and Pharmaceutical Sciences, Trinity College Dublin, Dublin 2, Ireland
[b] Department of Chemistry, Analytical and Biological Chemistry Research Facility, University College Cork, College Road, Cork, Ireland
[c] Department of Chemistry, Analytical and Biological Chemistry Research Facility and School of Pharmacy, University College Cork, College Road, Cork, Ireland

ARTICLE INFO

Article history:
Received 29 July 2011
Received in revised form 5 October 2011
Accepted 6 October 2011
Available online 13 October 2011

Keywords:
Intrinsic dissolution
Cocrystals
Solubility
Complexation
HPLC

ABSTRACT

This study examined the 1:1 cocrystal benzamide:dibenzyl sulfoxide, comprising the poorly water soluble dibenzyl sulfoxide (DBSO) and the more soluble benzamide (BA), to establish if this cocrystal shows advantages in terms of solubility and dissolution in comparison to its pure components and to a physical mixture. Solubility studies were performed by measuring DBSO solubility as a function of BA concentration, and a ternary phase diagram was constructed. Dissolution was examined through intrinsic dissolution studies. Solid-state characterisation was carried out by powder X-ray diffraction (PXRD), energy-dispersive X-ray diffraction (EDX), infra-red spectroscopy (ATR-FTIR) and thermal analysis. DBSO solubility was increased by means of complexation with BA. For the cocrystal, the solubility of both components was decreased in comparison to pure components. The cocrystal was identified as metastable and incongruently saturating. Dissolution studies revealed that dissolution of DBSO from the cocrystal was not enhanced in comparison to the pure compound or a physical mix, while BA release was retarded and followed square root of time kinetics. At the disk surface a layer of DBSO was found. The extent of complexation in solution can change the stability of the complex substantially. Incongruent solubility and dissolution behaviour of a cocrystal can result in no enhancement in the dissolution of the less soluble component and retardation of release of the more soluble component.

1. Introduction

Most active pharmaceutical ingredients (APIs) are available as solid oral dosage forms such as tablets or capsules and in this context the ability to deliver the drug to the patient is largely dependent on the dissolution properties of the API. One of the challenging tasks in the pharmaceutical industry is to design pharmaceutical solid materials with specific physicochemical properties (Besavoju et al., 2008). Solubility is one of the important parameters that have an impact on therapeutic effectiveness since it influences dissolution from dosage forms. Consequently, in the case of poorly water soluble drugs, low bioavailability is often observed after oral administration, since *in vivo* dissolution of drugs can be a rate-limiting step.

The formation of salts as an approach to alter solubility and dissolution properties of the API is well-known (Berge et al., 1977; Bighley et al., 1996; Machatha et al., 2005; Stahl and Wermuth, 2002). Formation of pharmaceutical cocrystals has gained attention offering another option that has the potential to provide new, stable solid structures which may improve the properties of the API and which is also applicable to non-ionizable drugs (Bailey Walsh et al., 2003; Schultheiss and Newman, 2009; Trask, 2007).

A number of cocrystals of APIs with different co-formers formed by different methods have been reported and it was shown that the solid-state interactions between the two compounds are mainly based on hydrogen bonds (Alhalaweh and Velaga, 2010; Childs et al., 2004; Lu and Rohani, 2009; Padrela et al., 2009; Paluch et al., 2011; Trask et al., 2005; Wenger and Bernstein, 2008). We have previously shown that the sulfoxide (S=O) functionality, common in a significant number of APIs, is a potent hydrogen bonding acceptor and forms cocrystals in association with a wide variety of amino (NH) functional groups (Eccles et al., 2010). The benzamide:dibenzyl sulfoxide (BA:DBSO) cocrystal, re-crystallised from toluene, with benzamide and dibenzyl sulfoxide in equimolar amounts is a representative example of this class. Dibenzyl sulfoxide acts as a hydrogen bond acceptor due to the polar sulfoxide moiety (Eccles et al., 2010) while being poorly water soluble, as is the case for a wide range of APIs. BA is a hydrogen bond donor with higher aqueous solubility in comparison to DBSO (O'Neil et al., 2006). Therefore, BA represents a model co-former of the cocrystal.

* Corresponding author. Tel.: +353 1 896 1444; fax: +353 1 896 2783.
E-mail address: healyam@tcd.ie (A.M. Healy).

0378-5173/$ – see front matter © 2011 Elsevier B.V. All rights reserved.
doi:10.1016/j.ijpharm.2011.10.016

Some cocrystals have previously been reported to result in improved bioavailabilty of poorly soluble APIs as a result of improved dissolution rate (Hickey et al., 2007; Jung et al., 2010; McNamara et al., 2006). Determination of the solubility of complexes was reported by Higuchi as early as in the 1950s (Higuchi and Connors, 1965). Rodríguez-Hornedo and co-workers have recently developed new theoretical models in order to predict solubility and solution stability of cocrystals (Good and Rodríguez-Hornedo, 2009, 2010; Nehm et al., 2006; Reddy et al., 2009). It was found that the solubility of cocrystals is strongly dependent on the co-former concentration in the appropriate solvent (Good and Rodríguez-Hornedo, 2009). Therefore, it is important to measure concentrations of both compounds when undertaking the solubility experiment. Solubility is a relevant parameter that has to be investigated for each cocrystal system since true equilibrium solubility might be difficult to measure due to solid-state transformation in solution (Good and Rodríguez-Hornedo, 2009). Such solution-mediated transformations to the thermodynamically more stable state should result in a change in the dissolution rate and therefore it is important to control/measure these processes. However, solid-state changes are not the sole rate-determining factors. Surface area, particle size distribution of the drug, fluid dynamics and the experimental apparatus can complicate the interpretation of dissolution results (Good and Rodríguez-Hornedo, 2009).

Intrinsic dissolution tests have been reported for numerous single component pharmaceutical materials (Avdeef and Tsinman, 2008; Higuchi et al., 1965; Mauger et al., 2003; O'Connor and Corrigan, 2001; Yu et al., 2004) whereas little literature is found for cocrystals (Childs et al., 2004; Jung et al., 2010; Lee et al., 2011; Rahman et al., 2011). The intrinsic dissolution rate is based on measurements of powder compacts of known surface area under conditions of controlled hydrodynamics (Healy et al., 2002) and is described as particle-size independent (Hendriksen and Williams, 1991; Wood et al., 1965). Since the surface area does not change over time, the dissolution rate depends on the solubility of the solute, hydrodynamics and diffusion coefficient in the dissolution medium (Hendriksen and Williams, 1991; Wood et al., 1965).

This report investigates solid-state characteristics, solubility and dissolution behaviour of the benzamide:dibenzyl sulfoxide cocrystal in comparison to its pure compounds and an equimolar physical mixture.

2. Materials and methods

2.1. Materials

Benzamide:dibenzyl sulfoxide (BA:DBSO) 1:1 cocrystal was synthesised as previously reported (Eccles et al., 2010); dibenzyl sulfoxide (DBSO) was synthesised as described by Kuliev et al. (1984), using dibenzyl sulfide which was purchased from Sigma–Aldrich (Ireland). Benzamide (BA) was also obtained from Sigma–Aldrich (Ireland). Acetonitrile, HPLC grade, was purchased from Fisher Scientific (Ireland) and water, ultra-pure, was prepared from an Elix 3 connected to Synergy UV system (Millipore, UK).

2.2. Methods

2.2.1. Powder X-ray diffraction (PXRD)

Powder X-ray analysis was performed using a Miniflex II Rigaku diffractometer with Ni-filtered Cu Kα radiation (λ = 1.54 Å). The tube voltage and tube current used were 30 kV and 15 mA, respectively. Each sample was scanned over a 2 theta range of 5–40° with a step size of 0.05°/s (Tajber et al., 2009). The program Mercury 2.3 was used for calculation of X-ray powder patterns on the basis of the single crystal structure established by Eccles et al. (2010).

2.2.2. Differential scanning calorimetry (DSC)

Differential scanning calorimetry was performed using a Mettler Toledo DSC 821^e instrument under nitrogen purge. Sample powders were placed in aluminium pans, sealed, pierced to provide three vent holes and heated at a rate of 10 °C/min in the temperature range of 25–250 °C (Tajber et al., 2005). Calibration of the instrument was carried out using indium as standard. The DSC system was controlled by Mettler Toledo STARe software (version 6.10) working on a Windows NT operating system.

2.2.3. Thermogravimetric analysis (TGA)

Thermogravimetric analysis was performed using a Mettler TG 50 module. Samples were placed into open aluminium pans (5–12 mg) and analysed at a constant heating rate of 10 °C/min under nitrogen purge (Tajber et al., 2005). The instrument was controlled by Mettler Toledo STARe software (version 6.10) working on a Windows NT operating system.

2.2.4. Attenuated total reflection Fourier transform infra-red spectroscopy (ATR-FTIR)

Infrared spectra were recorded on a PerkinElmer Spectrum 1 FT-IR Spectrometer and evaluated using Spectrum v5.0.1 software. Each spectrum was scanned in the range of 650–4000 cm^{-1} with a resolution of 4 cm^{-1} and a minimum of six scans were collected and averaged in order to gain good-quality spectra.

2.2.5. Equilibrium and dynamic solubility

The solubilities of pure compounds and cocrystal were determined using a 24-h shake flask method (used previously for many compounds) (Wermuth, 2008). Therefore, an excess of solid (approximately 2–3 times the amount expected to achieve saturation solubility) was added to 10 mL of water in glass ampoules, which were then heat sealed. To measure complexation between compounds, known amounts of BA of increasing concentration (= initial BA concentration) were dissolved in 10 mL of water in glass ampoules. Then excess (approximately 2–3 times the estimated solubility of the pure compound) of solid DBSO or cocrystal was added to each ampoule and the ampoules were heat sealed. The ampoules were placed horizontally in a thermostated water-bath at 37 °C and shaken at 100 cpm for 12 and 24 h and also at 48 and 72 h for dynamic solubility studies. After the appropriate time, the ampoules were opened, and the supernatant withdrawn and filtered through 0.45 μm membrane filters. Concentrations of the components in the supernatant were determined by HPLC as described below. We use the term "apparent solubility" to denote the solubility of systems where complexation occurs and "true" equilibrium solubility is therefore difficult to measure. The solid materials, remaining in the ampoule after 12 and 24 h of solubility studies were kept, dried at 40 °C and examined for phase transformation by PXRD, ATR-FTIR, DSC and TGA.

2.2.6. Transition concentration (C_{tr}) measurement

The transition concentration or invariant point was determined using a previously reported method (Good and Rodríguez-Hornedo, 2009). This was achieved by adding excess DBSO to a slightly undersaturated aqueous BA solution and by adding excess cocrystal to a presaturated aqueous DBSO solution. After 24 h supernatants were withdrawn, filtered through 0.45 μm membrane filters and quantified by HPLC as described below. C_{tr} values are expressed as the average established from these two experimental approaches (Good and Rodríguez-Hornedo, 2009). The solid phases were characterised by PXRD, ATR-FTIR, DSC and TGA.

2.2.7. Intrinsic dissolution study

The intrinsic dissolution rate (IDR) of solid materials was determined using constant surface area discs. These discs were prepared

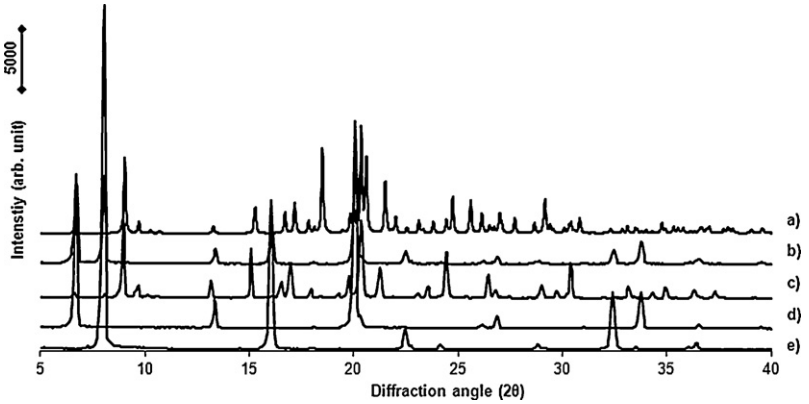

Fig. 1. PXRD patterns of (a) 1:1 BA:DBSO cocrystal calculated based on single crystal data, (b) BA:DBSO (1:1) physical mixture, (c) 1:1 BA:DBSO cocrystal, (d) pure DBSO and (e) pure BA.

by compressing powder into compacts using a PerkinElmer hydraulic press. Therefore, 300 mg of each solid was weighed and compressed in a 13 mm punch and die set at a pressure of 8 tonnes for 1.5 min. The compacts were coated using paraffin wax, leaving only the surface under investigation free for dissolution (Healy et al., 2002; Nicklasson et al., 1981) and affixed horizontally to the base of the dissolution vessel using adhesive tape. The stationary disc method was used in preference to the rotating disc method (Wood's apparatus). We have previously observed that, while the Wood apparatus is suitable for studying the dissolution of single component systems, it is less suited to multicomponent systems, with a greater tendency for disintegration and thus disruption of the constant surface area, than with the stationary disc method, which we have previously used successfully for two component systems (Healy and Corrigan, 1992, 1996).

The dissolution studies were carried out in ultra-pure, degassed water (volume: 900 mL, temperature: 37 °C) in a paddle apparatus (Apparatus 2, Ph. Eur.) at a rotation speed of 100 rpm. 5 mL aliquots were withdrawn (with replacement) at appropriate time intervals, filtered through 0.45 μm filters and analysed for sample content by HPLC at 254 nm under conditions as described below. The study, performed in triplicate, was terminated after 90 min. The IDR was determined from the slope of the dissolution time profiles. Initial and limiting rates were determined within the first 5 min and between 60 and 90 min, respectively. The discs were recovered, dried at ambient temperatures and then analysed by PXRD, ATR-FTIR and SEM/EDX for surface changes.

2.2.8. High Performance Liquid Chromatography (HPLC)

Concentrations of DBSO and BA in solutions were determined using a Shimadzu HPLC Class VP series with a LC-10AT VP pump, SIL-10AD VP autosampler and SCL-10VP system controller. The mobile phase was vacuum filtered through a 0.45 μm membrane filter (Gelman Supor-450). Separation was performed on a Luna C18 column (250 mm length, diameter 4.6 mm, particle size 5 μm) at a UV detection wavelength of 254 nm with an injection volume of 10 μL. The mobile phase consisted of acetonitrile/water 60/40 (v/v). The elution was carried out isocratically at ambient temperatures with a flow rate of 1 mL/min. For peak evaluation Class-VP 6.10 software was used.

2.2.9. Energy-Dispersive X-ray (EDX) analysis and Scanning Electron Microscopy (SEM)

In order to determine the elemental composition on compact surfaces, EDX analysis was performed using a Tescan Mira Variable Pressure Field Emission Scanning Electron Microscope (Czech Republic), operating at a resolution of 3 nm at 30 kV and equipped with an Oxford Inca energy-dispersive microprobe and a backscattered electron detector. Powder compacts were glued onto aluminium stubs using carbon cement, dried for 24 h at ambient temperatures and coated with carbon under vacuum prior to analysis. X-ray spectra were evaluated quantitatively on the basis of the carbon peak. Furthermore, surface images at various magnifications were performed by SEM using a Zeiss Supra Variable Pressure Field Emission Scanning Electron Microscope (Germany) at a resolution of 1.5 nm at 15 kV equipped with a secondary electron detector. Powder compacts were glued onto aluminium stubs using carbon cement, dried for 24 h at ambient temperatures and sputter-coated with gold under vacuum prior to analysis.

2.2.10. Two sample t-test

Microsoft Excel data analysis software was used to determine statistical significance. The two sample *t*-test was used to compare the means and standard deviations of two independent samples at a significance level of $\alpha = 0.05$.

2.2.11. Linear regression

Linear regression analysis was performed using the method of least squares by Microsoft Excel software. The adequacy of the fit was assessed from the regression coefficient (R^2).

3. Results and discussion

3.1. Solid-state properties

The powder X-ray diffraction pattern of the 1:1 BA:DBSO cocrystal is shown in Fig. 1. This revealed a characteristic diffraction pattern, which differed from those of the two individual components (DBSO and BA) and the equimolar physical mixture. The DSC thermogram in Fig. 2 confirmed the presence of the cocrystal and indicated a sharp endothermic melting event with an onset temperature of around 115 °C (with a heat of fusion, $\Delta H_f = 161$ J/g). In contrast BA and DBSO, showed melting onsets at around 127 °C ($\Delta H_f = 186$ J/g) and 135 °C ($\Delta H_f = 132$ J/g), respectively.

ATR-FTIR revealed evidence of significant intermolecular interactions based on two characteristic shifts towards lower frequencies. As shown in Fig. 3, the symmetric NH stretching band of BA is shifted from 3173 cm^{-1} to 3140 cm^{-1} and the S=O functional group from 1032 cm^{-1} to 1013 cm^{-1}. These shifts were not observed for the physical mixture.

The reason for these shifts of IR bands was explained based on the single crystal X-ray diffraction data previously reported for the 1:1 BA:DBSO cocrystal which showed that molecular association between BA and DBSO occurs through hydrogen bonding (Eccles

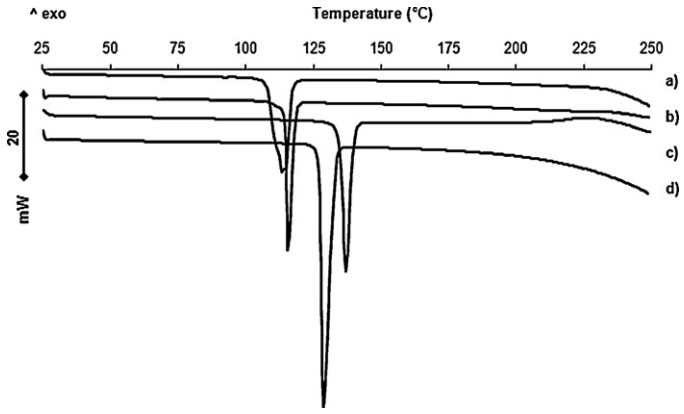

Fig. 2. DSC thermograms of (a) BA:DBSO (1:1) physical mixture, (b) 1:1 BA:DBSO cocrystal, (c) pure DBSO and (d) pure BA.

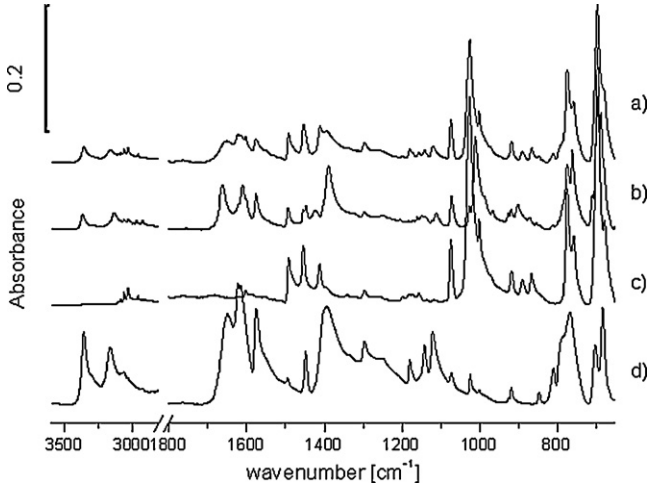

Fig. 3. FTIR spectra of (a) BA:DBSO (1:1) physical mixture, (b) 1:1 BA:DBSO cocrystal, (c) pure DBSO and (d) pure BA.

et al., 2010). Generation of the theoretical PXRD diffractogram from the single crystal data (Fig. 1a) showed consistency with the experimental PXRD pattern of the cocrystal (Fig. 1c).

3.2. Solubility study

The solubilities for BA and DBSO in water at 37 °C were found to be 13.1 ± 0.20 mg/mL ($0.11 \pm 1.67 \times 10^{-3}$ mmol/mL) and 0.33 ± 0.01 mg/mL ($1.43 \times 10^{-3} \pm 2.74 \times 10^{-5}$ mmol/mL), respectively (Table 1). The apparent solubility of the cocrystal in water at 37 °C was determined by measuring DBSO and BA concentrations and values of 3.07 ± 0.18 mg/mL ($2.54 \times 10^{-2} \pm 1.48 \times 10^{-3}$ mmol/mL) for BA and 0.27 ± 0.01 mg/mL ($1.18 \times 10^{-3} \pm 4.51 \times 10^{-5}$ mmol/mL) for DBSO were obtained (Table 1). These results show that the apparent solubilities of

Table 1
Solubility/apparent solubility of pure compounds, co-mixed and cocrystallised BA and DBSO.

Substance	Description	Solubility (mg/mL)	Solubility (mmol/mL)
Benzamide	Pure material	13.1 ± 0.202	$0.108 \pm 1.67 \times 10^{-3}$
	Physical mixture	$9.40 \pm 0.165 \times 10^{-2}$	$7.76 \times 10^{-2} \pm 1.36 \times 10^{-3}$
	Cocrystal	3.07 ± 0.179	$2.54 \times 10^{-2} \pm 1.48 \times 10^{-3}$
DBSO	Pure material	$0.330 \pm 6.30 \times 10^{-3}$	$1.43 \times 10^{-3} \pm 2.74 \times 10^{-5}$
	Physical mixture	$0.324 \pm 2.43 \times 10^{-3}$	$1.41 \times 10^{-3} \pm 1.06 \times 10^{-5}$
	Cocrystal	$0.273 \pm 1.04 \times 10^{-2}$	$1.18 \times 10^{-3} \pm 4.51 \times 10^{-5}$

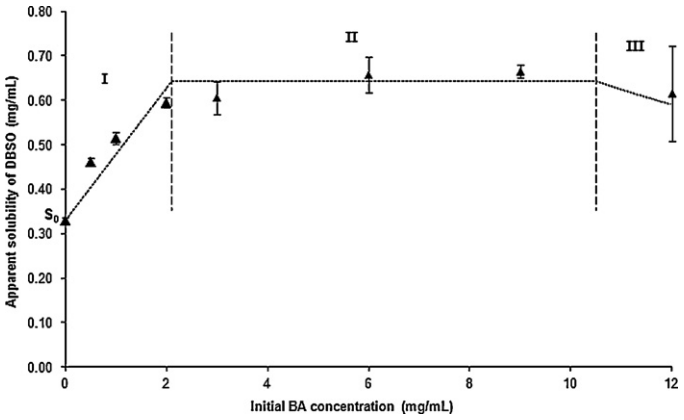

Fig. 4. Profile of the apparent solubility of DBSO (mg/mL) as a function of BA concentration measured after 24 h. S_0 is the DBSO concentration in absence of BA. The dashed lines confirm the behaviour of a Type B phase solubility diagram illustrating region I (solution complexation), II (conversion to complex and precipitation) and III (decreased solubility of precipitated complex with increasing BA in solution).

the cocrystal components were decreased in comparison to the solubilities of the pure compounds.

The apparent solubilities of DBSO and cocrystal were measured as a function of co-former (BA) concentration in order to determine solution complexation. Investigation of solution interactions revealed that the apparent solubility of DBSO initially increased with increasing concentration of BA, when DBSO was the excess phase, due to soluble complex formation between the two compounds (Fig. 4). The solubility profile of DBSO with increasing BA concentration can be described as a Type B phase-solubility diagram (Higuchi and Connors, 1965). When the concentration of BA initially was ≥3 mg/mL the solubility limit of the complex formed was exceeded and uncomplexed DBSO in solution did not change significantly, as shown by the plateau in Fig. 4. In this context, the increase in the apparent DBSO solubility i.e. the amount of DBSO that enters into soluble complex formation was determined (Higuchi and Connors, 1965). A nearly two-fold increase in the apparent DBSO solubility in the presence of BA, in comparison to DBSO solubility in water alone, was observed.

Precipitation of the complex was apparent on PXRD analysis of the solid residue which indicated the presence of two phases, cocrystal and DBSO. When the initial BA concentration was 12 mg/mL, and therefore close to its aqueous solubility, nearly all solid DBSO was consumed leading to depletion of DBSO, followed by complex precipitation induced by supersaturation of the solution. The precipitated solid phase was cocrystal contaminated with DBSO (Fig. 5).

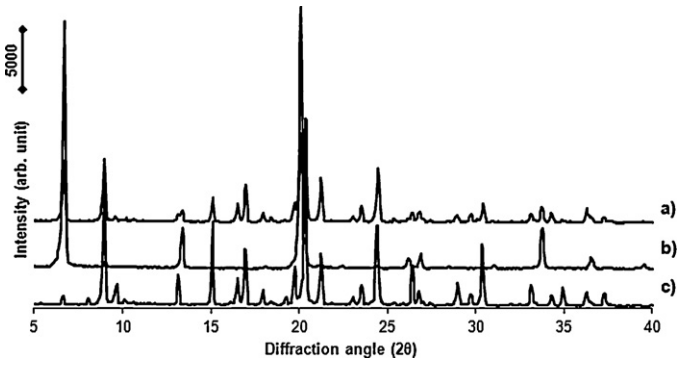

Fig. 5. PXRD patterns of (a) remaining solid (12 mg/mL BA added) after 24 h solubility study, (b) remaining solid (12 mg/mL BA added) after 12 h solubility study, (c) 1:1 BA:DBSO cocrystal.

Furthermore, a significant decrease in the apparent DBSO solubility after 24 h in comparison to 12 h was observed at 12 mg/mL BA in solution. PXRD analysis of the remaining solid material revealed that this decrease in solubility reflected cocrystal formation and subsequent precipitation, since the diffraction pattern of the solid residue is superimposable on that of the cocrystal re-crystallised from toluene (Fig. 5).

The increase in the apparent solubility of DBSO in the presence of BA can be expressed by a complex formation (or stability) constant (Higuchi and Connors, 1965). For 1:1 soluble complexes, this constant is given by Eq. (1):

$$K_{11} = \frac{[AB]}{[A][B]} \quad (1)$$

where [A] and [B] are the (molar) concentrations of each component at equilibrium. Thus the increase in solubility may be quantified (Eq. (2)):

$$[A]_T = \frac{K_{11}[A]_0[B]_T}{1 + K_{11}[A]_0} + [A]_0 \quad (2)$$

where $[A]_T$ is the total concentration of dissolved A, $[A]_0$ is the equilibrium solubility of A in the absence of B and $[B]_T$ is the total added concentration of B. Assuming that compounds A and B are DBSO and BA, respectively, a plot of the total concentration of DBSO in solution against the total concentration of BA in solution enables the stability constant, K_{11}, to be determined from the slope of the line using Eq. (3) (Higuchi and Connors, 1965) (data shown in Fig. 4, best fit 0–2 mg/mL).

$$K_{11} = \frac{\text{slope}}{[A]_0(1 - \text{slope})} \quad (3)$$

Assuming the formation of a single soluble complex, a value of $K_{11} = 55.7 \pm 2.92\ M^{-1}$ was calculated (Table 1).

In studies where the cocrystal was the excess phase, a different solubility profile was observed. Although the apparent DBSO solubility increased initially with increasing BA concentration, a significant continuous decrease in DBSO concentration associated with precipitation of the cocrystal, confirmed by PXRD, ATR-FTIR and DSC/TGA, as the sole remaining solid phase was observed at initial BA concentrations of ≥6 mg/mL BA (Fig. 6). The data suggests that the soluble complex reached a solubility limit when the initial BA concentration was >3 mg/mL BA (Fig. 6).

A dynamic solubility profile, obtained on a sample containing initially 6 mg/mL BA and excess of the cocrystal, is shown in Fig. 7. It is evident that, after 24 h a maximum apparent DBSO solubility was reached followed by a significant decrease in DBSO concentration. Analysis of the solid residue for the ≥24 h timepoints indicated the presence of only the cocrystal phase. Thus the decrease in DBSO concentration was associated with cocrystal precipitation.

Furthermore, the apparent DBSO solubilities, where the cocrystal was the excess phase, were found to be significantly lower than those obtained from samples containing DBSO as the excess phase (Figs. 4 and 6).

To describe the solubility of binary cocrystals considering the equilibrium between cocrystal and cocrystal components in solution, various equations have been developed. Complex formation in solution of a 1:1 stoichiometric cocrystal is described by

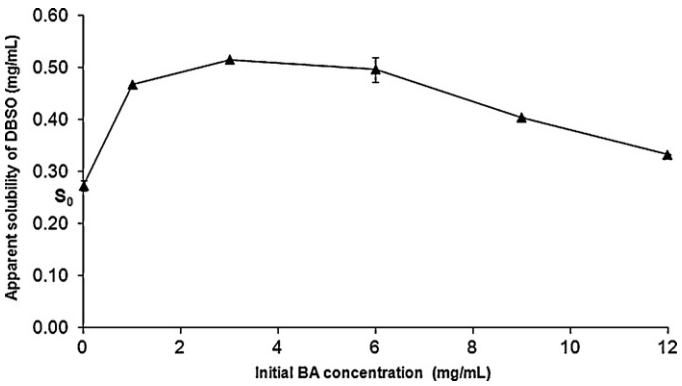

Fig. 6. Solubility profile of DBSO after 24 h where cocrystal is the excess phase in dependency of BA. S_0 represents the DBSO concentration in the absence of BA.

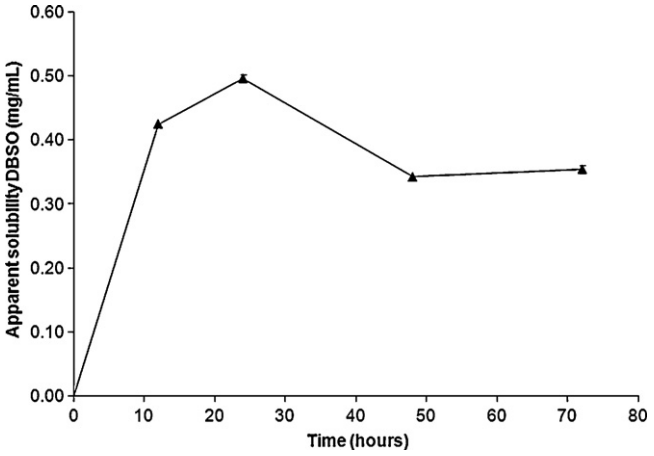

Fig. 7. Dynamic solubility profile of DBSO from cocrystal in presence of 6 mg/mL BA over 72 h.

two constants (Nehm et al., 2006); firstly the cocrystal solubility product, K_{sp} (Eq. (4)), which reflects the strength of cocrystal solid-state interactions of component *A* and component *B* relative to interactions with the solvent, where [A] and [B] are the molar concentrations of each cocrystal component at equilibrium, and the superscripts, α and β, refer to the stoichiometric number of molecules of A and B in the complex (Nehm et al., 2006) and secondly the binding constant for a 1:1 complex formed in solution, K_{11}, as described by Eq. (5) or (1).

$$K_{sp} = [A]^{\alpha}[B]^{\beta} \quad (4)$$

$$K_{11} = \frac{[AB]}{[A][B]} = \frac{[AB]}{K_{sp}} \quad (5)$$

Combining Eqs. (4) and (5) leads to Eq. (6) (Nehm et al., 2006), where cocrystal solubility can be expressed in terms of the total ligand concentration $[B]_T$:

$$[A]_T = \frac{K_{sp}}{[B]_T} + K_{11}K_{sp} \quad (6)$$

Table 2
Estimated constants calculated from solubility data.

Calculation of parameter based on	Determined parameter	Result	Regression coefficient
API solubility as a function of ligand	K_{11}	$55.7 \pm 2.92\ M^{-1}$	0.83
Cocrystal solubility as a function of ligand	K_{sp} K_{11}	$3.90 \times 10^{-5} \pm 3.64 \times 10^{-6}\ M^2$ $30.5 \pm 2.54\ M^{-1}$	0.95
Transition concentration	K_{sp}	$1.05 \times 10^{-4} \pm 1.24 \times 10^{-7}\ M^2$	–

Therefore a plot of $[A]_T$ versus $1/[B]_T$ enables K_{sp} and K_{11} to be determined from the slope and the intercept, provided that no higher order complexes are formed in solution (Nehm et al., 2006). For the 1:1 BA:DBSO cocrystal, a solubility product of $K_{sp} = 3.90 \times 10^{-5} \pm 3.64 \times 10^{-6}$ M^2 and a solution complexation constant of $K_{11} = 30.53 \pm 2.54\ M^{-1}$ were estimated (Table 2). The K_{11} in this case was quite high compared to previously reported values for cocrystals (Nehm et al., 2006) (Table 2) as a result of the compound's low solubility (K_{11} is inversely related to K_{sp}). Strong solute–solute interactions in water at 37 °C are expected, which is reflected in the high stability of the complex in solution (Good and Rodríguez-Hornedo, 2009).

In order to control crystallisation of cocrystals in solution, predict phase transformations and therefore determine the thermodynamic stability of individual cocrystal systems, another parameter, the so-called transition concentration or eutectic concentration, C_{tr}, which defines the thermodynamic stability of either the solid cocrystal or DBSO, is relevant (Good and Rodríguez-Hornedo, 2009).

The transition concentration can also be used to determine cocrystal solubility, in particular for incongruently saturating cocrystals, which are termed metastable and for which equilibrium solubility is difficult to measure since it is possible that drug going into solution can be followed by crystallisation because of supersaturation (Good and Rodríguez-Hornedo, 2009).

Based on the solubility obtained for the 1:1 BA:DBSO cocrystal, the molar ratio of DBSO to BA in solution was found to be 0.05:1 indicating that the system is incongruently saturating.

The dashed line in Fig. 8 represents stoichiometric concentrations of cocrystal components assuming that the 1:1 BA:DBSO cocrystal is congruently saturating, and its intersection with the cocrystal equilibrium curve indicates the theoretical maximum drug concentration attributed to cocrystal solubility (Good and Rodríguez-Hornedo, 2009).

For metastable cocrystals this intersection lies above the solubility of the pure drug (Good and Rodríguez-Hornedo, 2009) and implies that the cocrystal should be more soluble than the drug

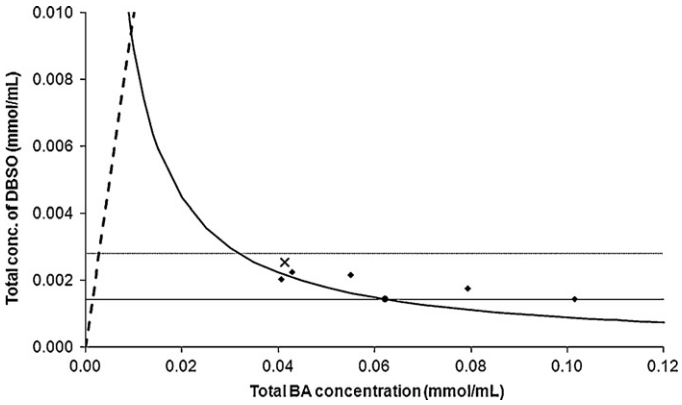

Fig. 8. Phase solubility diagram of 1:1 BA:DBSO cocrystal. The horizontal line marks the solubility of pure DBSO, the curved line represents the cocrystal solubility curve determined by Eq. (3), the dotted line represents the solubility limit of complex as determined from the plot presented in Fig. 4, the filled diamonds mark the experimental cocrystal solubility values (BA dependent), the dashed line represents stoichiometric concentrations of cocrystal components that dissolution could follow in the ideal case, the filled circle symbolises the transition concentration (DBSO/CC) and the cross illustrates the experimentally obtained transition concentration (DBSO/CC).

provided that no component precipitation occurs. This theoretical increase in DBSO solubility when formulated as the DBSO:BA cocrystal was calculated to be approximately 7-fold compared to the solubility of DBSO alone.

A transition concentration (C_{tr}) of $4.14 \times 10^{-2} \pm 1.20 \times 10^{-3}$ mmol/mL for BA and $2.54 \times 10^{-3} \pm 1.03 \times 10^{-4}$ mmol/mL for DBSO at the eutectic composition of cocrystal/DBSO was determined and is presented in Fig. 8. From these concentrations, a cocrystal solubility product with a value of $1.05 \times 10^{-4} \pm 1.24 \times 10^{-7}$ M^2 (Table 2) was calculated and the molar ratio of BA:DBSO at C_{tr} of 1:0.06 (BA:DBSO) was found, which is similar to the molar BA:DBSO solubility ratio measured for the pure cocrystal. A comparison of the K_{sp} values obtained from transition concentrations and calculated from

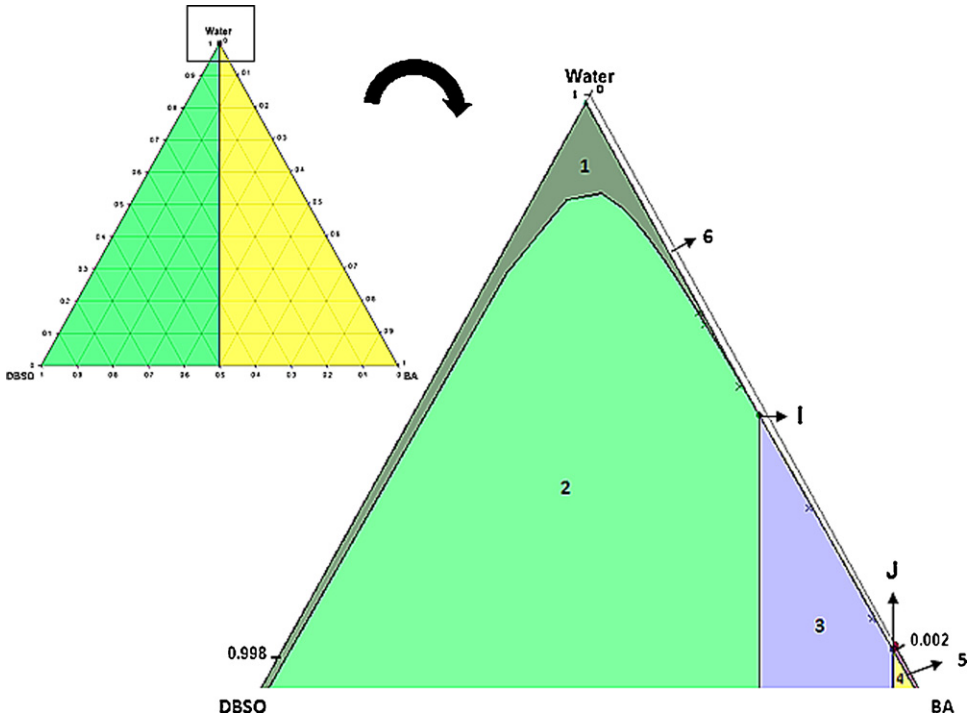

Fig. 9. Zoom and downscaled view of ternary phase diagram of 1:1 BA:DBSO cocrystal in water at 37 °C (in mole fractions).

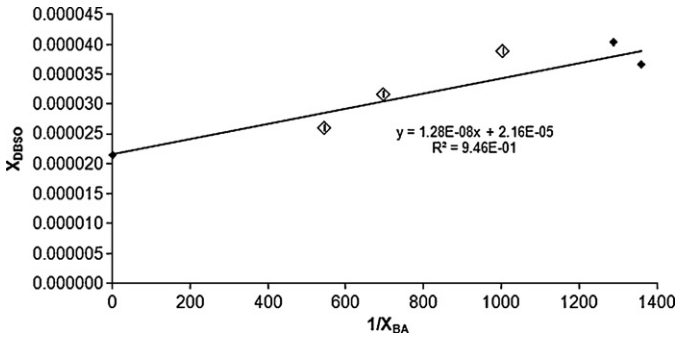

Fig. 10. DBSO in equilibrium with cocrystal (closed diamonds) as a function of the inverse total BA concentration at 37 °C (in molar fractions). Open diamonds represent solubility data beyond the equilibrium state. Trendline refers to closed diamonds.

equilibrium cocrystal solubility revealed that the former is two-fold higher (Table 2). The difference in K_{sp} values may be explained by solution complexation as solubility products based on transition concentrations do not account for solution complexation of cocrystal components (Good and Rodríguez-Hornedo, 2009).

The DBSO transition concentration was close to the DBSO solubility induced by solution complexation (dotted line, Fig. 8). We can therefore assume that strong solute–solute interactions which are attributed to a high complexation constant (K_{11}), can shift the DBSO transition concentration to higher values and can thus increase cocrystal stability, which reduces the risk of API crystallisation. However, if the affinity of API and co-former in solution is stronger than the affinity to the solvent, the solubility of the API and consequently dissolution is likely to be reduced.

3.3. Ternary phase diagram

A three-component phase diagram of the benzamide:dibenzyl sulfoxide cocrystal in water at 37 °C was constructed, based on methods previously described (Ainouz et al., 2009; Chiarella et al., 2007; Nehm et al., 2006), and is shown in Fig. 9. The cocrystal solution equilibrium is described by

$$K_{app} = X_A^{\alpha} \times X_B^{\beta} \quad (7)$$

where K_{app} is the apparent constant and X_A^{α} and X_B^{β} are the molar fractions of the API and co-former in stoichiometric ratio, respectively (Ainouz et al., 2009). Plotting X_A versus $1/X_B$ allows K_{app} to be calculated from the slope of the line and K_{app} is therefore regarded as equivalent to K_{sp} determined from the component concentrations as previously described.

Fig. 10 illustrates the X_A versus $1/X_B$ relationship for 1:1 BA:DBSO cocrystal leading to a K_{app} of 1.28×10^{-8}. This value was then used to model the cocrystal equilibrium line as seen in Fig. 9.

The DBSO–liquid equilibrium line and BA–liquid equilibrium line, respectively, are illustrated based on the molar fractions of the respective binary solubilities (Fig. 9). The numbers (1–6) describe the region of the appropriate stable solid phase(s) and the black lines illustrate the solid–liquid equilibrium curves. The curved line displays the solid–liquid equilibrium of the cocrystal and the points, labelled by a cross (X), are experimental data points. The following solid phases were found to be stable in the marked zones: pure DBSO in zone 1, DBSO and cocrystal in zone 2, cocrystal in zone 3, BA and cocrystal in zone 4 and pure BA in zone 5, respectively. Zone 6 is the undersaturated solution phase where all three compounds are present and points I and J symbolise the eutectic mixtures of DBSO/cocrystal and BA/cocrystal, respectively.

The asymmetric shape of the different zones is consistent with the incongruent solubility behaviour of the 1:1 BA:DBSO cocrystal since the homogenous liquid phase (zone 6) and cocrystal phase

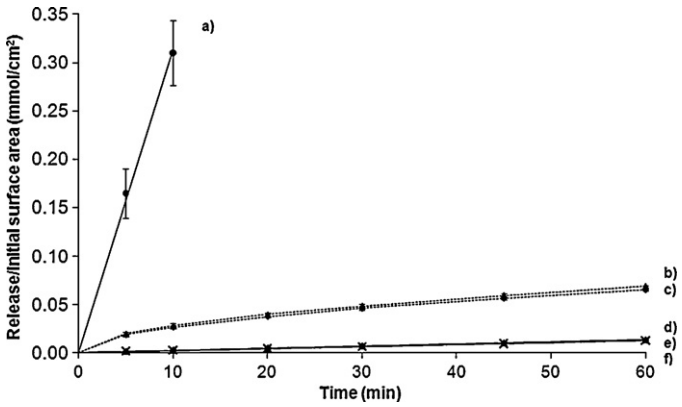

Fig. 11. Dissolution profiles of (a) BA, (b) BA from a physical mixture, (c) BA from the cocrystal, (d) DBSO from a physical mixture, (e) DBSO from the cocrystal and (f) DBSO. The dashed line refers to the square-root of time fit.

(zone 3) are very small and shifted to the right of the diagram (Ainouz et al., 2009). Even though the solubilities of BA and DBSO in water are low and zone 3 very asymmetric, it is still possible to isolate the cocrystal from water, consistent with our experimental observations.

From these results, showing incongruent apparent solubility of the 1:1 BA:DBSO cocrystal in water at 37 °C, it is expected that BA and DBSO from the cocrystal will dissolve incongruently.

3.4. Dissolution rate studies

Intrinsic dissolution profiles from compacts of the 1:1 BA:DBSO cocrystal and an equimolar physical mixture of DBSO and BA as well as the pure compounds in water at 37 °C are shown in Fig. 11. BA dissolved much more rapidly than DBSO, consistent with the solubility differences. BA dissolution from the equimolar physical mix was initially more rapid than from the cocrystal and both profiles were nonlinear, the rates declining over time. Based on the initial dissolution rate, pure BA dissolved approximately 7 times faster than when physically mixed with DBSO and approximately 12 times faster than BA from the cocrystal. Furthermore the dissolution rates of BA from the cocrystal and the physical mixture appeared to converge (Table 3, limiting rate). In contrast, DBSO profiles were linear and gave similar intrinsic dissolution rates ($R^2 > 0.96$) in all cases (Table 3).

The dissolution from the physical mix compact was qualitatively consistent with that expected for dissolving polyphase mixtures (Higuchi et al., 1965) when the more soluble component dissolves more rapidly from the surface of a compact, leaving a porous layer of the less soluble component behind.

Table 3
Dissolution rates (mmol/min/cm²) of pure BA and pure, co-mixed and cocrystallised DBSO.

Substance	Description	IDR (mmol/min/cm²)
BA	Pure material	$3.95 \times 10^{-2} \pm 6.83 \times 10^{-3}$ [a,*]
		$8.75 \times 10^{-3} \pm 1.46 \times 10^{-4}$ [b,*]
	Physical mixture	$5.74 \times 10^{-3} \pm 6.36 \times 10^{-4}$ [a,*]
		$5.65 \times 10^{-4} \pm 8.17 \times 10^{-6}$ [b,*]
	Cocrystal	$3.19 \times 10^{-3} \pm 9.92 \times 10^{-5}$ [a,*]
		$4.91 \times 10^{-4} \pm 2.74 \times 10^{-5}$ [b,*]
DBSO	Pure material	$2.14 \times 10^{-4} \pm 3.50 \times 10^{-5}$ [**]
	Physical mixture	$2.20 \times 10^{-4} \pm 1.32 \times 10^{-5}$ [**]
	Cocrystal	$2.29 \times 10^{-4} \pm 3.07 \times 10^{-7}$ [**]

[a] Initial dissolution rate.
[b] Limiting dissolution rate.
[*] Significantly different ($p < 0.05$).
[**] Not significantly different ($p > 0.05$).

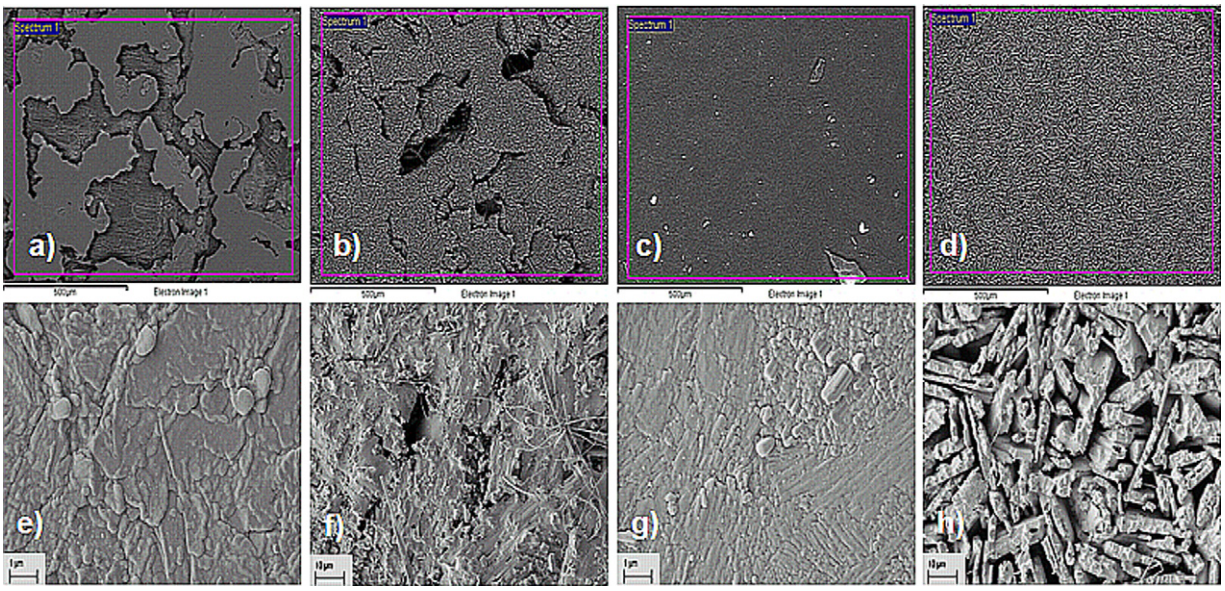

Fig. 12. Backscattered electron images of solid compacts of (a) BA:DBSO (1:1) physical mixture before dissolution, (b) BA:DBSO (1:1) physical mixture after dissolution, (c) 1:1 BA:DBSO cocrystal before dissolution and (d) 1:1 BA:DBSO cocrystal after dissolution and secondary electron images of (e) BA:DBSO (1:1) physical mixture before dissolution, (f) BA:DBSO (1:1) physical mixture after dissolution, (g) 1:1 BA:DBSO cocrystal before dissolution and (h) 1:1 BA:DBSO cocrystal after dissolution.

Table 4
Sulfur content found on the compact surface, before and after dissolution, by energy-dispersive X-ray (EDX) analysis.

Sample	Sulfur content (%, wt.)
DBSO	
(a) Before dissolution	14.4 ± 0.503
(b) After dissolution	13.7 ± 0.372
Physical mixture	
(a) Before dissolution	10.3 ± 0.0141
(b) After dissolution	13.3 ± 0.259
Cocrystal	
(a) Before dissolution	10.2 ± 0.0870
(b) After dissolution	13.2 ± 0.247

Energy-dispersive X-ray (EDX) analysis was used to determine the elemental composition of the sample surfaces and revealed that the surface of the cocrystal and the equimolar physical mixture contained a similar amount of sulfur after the 90 min dissolution experiments. The same was observed before dissolution; however, the sulfur content was significantly lower compared to that after dissolution (Table 4). Furthermore, both samples after dissolution showed sulfur contents which were nearly equal to that detected for pure DBSO discs. The percentage of sulfur is calculated relative to the amount of carbon and thus, the sulfur content is expected to be lower when both organic components, BA and DBSO, are present at the surface, as is the case prior to dissolution. The faster dissolution of the more soluble BA leaving the less soluble DBSO at the surface results in higher sulfur content on the surface of the disc, as confirmed by the EDX results (Table 4). Additionally, backscattered electronic images displayed differences in the surface structure between the cocrystal and physical mixture (Fig. 12). The physical mixture showed an inhomogeneous compact surface with randomly positioned holes in the surface after dissolution, attributed to the dissolution of BA. In contrast, the cocrystal displayed a rather homogenous surface and after dissolution an ordered surface structure, presumed to be as a result of BA release (Fig. 12a–d). These results were consistent with the SEM images using a secondary electron detector and a 5–50 times higher magnification (Fig. 12e–h).

Calculated dissolution rates for polyphase mixtures under steady state conditions require that the solubilities of A and B do not differ by more than a factor of about 100 for the case of a compact thickness of the order of millimetres (Higuchi, 1967). Since the solubility ratio of BA/DBSO (in mmol/mL) is large with a value of approximately 75, and the more soluble BA is present with a lower weight fraction (34%), it was expected that the steady state assumptions were not applicable (Higuchi et al., 1965) and consequently, solute release for the more soluble component is better described as from an inert matrix system (Higuchi, 1967), where the more soluble component dissolves through a matrix of the less soluble component. The BA release was found to be diffusion controlled and directly proportional to the square root of time ($R^2 > 0.99$) (Higuchi, 1963) (Fig. 11).

From these dissolution results we can conclude, that the extent of solution complexation between DBSO and BA is not sufficient to enhance dissolution of the less soluble DBSO, either when physically mixed or in the cocrystallised form. The solubility and dissolution of BA are found to be controlled by, and suppressed in the presence of, DBSO.

4. Conclusion

Solubility studies on the 1:1 BA:DBSO cocrystal revealed that the apparent solubility of DBSO was increased due to solution complexation while the apparent solubility of BA was significantly decreased. Furthermore, it was found that the 1:1 BA:DBSO cocrystal is metastable and incongruently saturating as evidenced by the asymmetric phase behaviour of the ternary phase diagram.

Investigation of the intrinsic dissolution rate confirmed, as expected from the solubility tests, that BA and DBSO dissolved incongruently and that the dissolution of the cocrystal was not enhanced in comparison to an equimolar physical mixture and the pure components.

The co-former compound, BA, dissolved initially faster when mixed than when cocrystallised with DBSO, which is assumed due to stronger solid-state attractive forces between the amino and sulfoxide group in the form of hydrogen bonds on the surface of the compact for the cocrystal. However, for both forms, cocrystal

and physical mixture, we found that the surface of the compacts contained only DBSO after dissolution.

Based on dissolution models for compressed physical mixtures, it was apparent that steady-state conditions were not reached in the dissolution experiment as a result of the large solubility difference between BA and DBSO in water. Furthermore, we could demonstrate that DBSO controls and retards dissolution of BA and becomes the phase remaining at the surface independent of the initial solid-state form.

Consequently, the more soluble BA is not a suitable cocrystal component to improve the solubility and dissolution of the poorly soluble DBSO. In this context, complexation in solution is a factor that can influence the solubility and dissolution substantially and is therefore important to measure. In order to enhance solubility and dissolution of the API from a cocrystal complex, a compromise between solid-state, solute–solute and solute–solution stability needs to be found.

Acknowledgement

The authors gratefully acknowledge J.-R. Authelin and P. Billot from Sanofi Aventis for their advice and help concerning ternary phase diagram and N. Maguire from the Chemistry Department in University College Cork for developing the HPLC method. This publication has emanated from research conducted with the financial support of Science Foundation Ireland, under grant numbers 07/SRC/B1158 (Solid State Pharmaceutical Cluster) and 08/RFP/MTR1664.

References

Ainouz, A., Authelin, J.-R., Billot, P., Lieberman, H., 2009. Modeling and prediction of cocrystal phase diagrams. Int. J. Pharm. 374, 82–89.

Alhalaweh, A., Velaga, S.P., 2010. Formation of cocrystals from stoichiometric solutions of incongruently saturating systems by spray drying. Cryst. Growth Des. 10, 3302–3305.

Avdeef, A., Tsinman, O., 2008. Miniaturized rotating disk intrinsic dissolution rate measurement: effects of buffer capacity in comparisons to traditional wood's apparatus. Pharm. Res. 25, 2613–2627.

Bailey Walsh, R.D., Bradner, M.W., Fleischman, S., Morales, L.A., Moulton, B., Rodríguez-Hornedo, N., Zaworotko, M.J., 2003. Crystal engineering of the composition of pharmaceutical phases. Chem. Commun. 9, 186–187.

Berge, S.M., Bighley, L.D., Monkhouse, D.C., 1977. Pharmaceutical salts. J. Pharm. Sci. 66, 1–19.

Besavoju, S., Bostroem, D., Velaga, S.P., 2008. Indomethacin–saccharin cocrystal: design, synthesis and preliminary pharmaceutical characterization. Pharm. Res. 25, 530–541.

Bighley, L.D., Berge, S.M., Monkhouse, D.C., 1996. Presevation of pharmacuetical products to salt forms of drugs and absorption. In: Swarbrick, J., Boylan, J.C. (Eds.), Encycolpedia of Pharmaceutical Technology, vol. 13. Marcel Dekker, New York, pp. 453–499.

Chiarella, R.A., Davey, R.J., Peterson, M.L., 2007. Making co-crystals—the utility of ternary phase diagrams. Cryst. Growth Des. 7, 1223–1226.

Childs, S.L., Chyall, L.J., Dunlap, J.T., Smolenskaya, V.N., Stahly, B.C., Stahly, G.P., 2004. Crystal engineering approach to forming cocrystals of amine hydrochlorides with organic acids. Molecular complexes of fluoxetine hydrochloride with benzoic, succinic and fumaric acids. J. Am. Chem. Soc. 126, 13335–13342.

Eccles, K.S., Elcoate, C.J., Stokes, S.P., Maguire, A.R., Lawrence, S.E., 2010. Sulfoxides: potent co-crystal formers. Cryst. Growth Des. 10, 4243–4245.

Good, D.J., Rodríguez-Hornedo, N., 2009. Solubility advantage of pharmaceutical cocrystals. Cryst. Growth Des. 9, 2252–2264.

Good, D.J., Rodríguez-Hornedo, N., 2010. Cocrystal eutectic constants and prediction of solubility behavior. Cryst. Growth Des. 10, 1028–1032.

Healy, A.M., Corrigan, O.I., 1992. Predicting the dissolution rate of ibuprofen-acidic excipient compressed mixtures in reactive media. Int. J. Pharm. 84, 167–173.

Healy, A.M., Corrigan, O.I., 1996. The influence of excipient particle size, solubility and acid strength on the dissolution of an acidic drug from two-component compacts. Int. J. Pharm. 143, 211–221.

Healy, A.M., McCarthy, L.G., Gallagher, K.M., Corrigan, O.I., 2002. Sensitivity of dissolution rate to location in the paddle dissolution apparatus. J. Pharm. Pharmacol. 54, 441–444.

Hendriksen, B.A., Williams, J.D., 1991. Characterization of calcium fenoprofen 2. Dissolution from formulated tablets and compressed rotating discs. Int. J. Pharm. 69, 175–180.

Hickey, M.B., Peterson, M.L., Scoppettuolo, L.A., Morrisette, S.L., Vetter, A., Guzman, H., Remenar, J.F., Zhang, Z., Tawa, M.D., Haley, S., Zaworotko, M.J., Almarsson, O., 2007. Performance comparison of a co-crystal of carbamazepine with marketed product. Eur. J. Pharm. Biopharm. 67, 112–119.

Higuchi, T., 1963. Mechanism of sustained-action medication. Theorectical analysis of rate. J. Pharm. Sci. 52, 1145–1149.

Higuchi, T., Connors, K.A., 1965. Phase solubility techniques. Adv. Anal. Chem. Instrum. 4, 117–212.

Higuchi, W.I., Mir, N.A., Desai, S.J., 1965. Dissolution rates of polyphase mixtures. J. Pharm. Sci. 54, 1405–1410.

Higuchi, W.I., 1967. Diffusional models useful in biopharmaceutics. Drug release rate processes. Pharm. Sci. 56, 315–324.

Jung, M.S., Kim, J.S., Kim, M.S., Alhalaweh, A., Cho, W., Hwang, S.J., Velaga, S.P., 2010. Bioavailability of indomethacin–saccharin cocrystals. J. Pharm. Pharmacol. 62, 1560–1568.

Kuliev, F.A., Aslanov, A.D., Denisov, E.T., 1984. Synthesis and spectra of dibenzyl sulfoxides and sulfones. Azerbaidzhanskii Khimicheskii Zhurnal 1, 72–75.

Lee, H.-G., Zhang, G.G.Z., Flanagan, D.R., 2011. Cocrystal intrinsic dissolution behavior using a rotating disk. J. Pharm. Sci. 100, 1736–1744.

Lu, J., Rohani, S., 2009. Preparation and characterization of theophylline–nicotinamide cocrystal. Org. Process Res. Dev. 13, 1269–1275.

Machatha, S.G., Sanghvi, T., Yalkowsky, S.H., 2005. Structure determination and characterization of carbendazim hydrochloride dihydrate. AAPS Pharm. Sci. Tech. 6, E115–E119.

Mauger, J., Ballard, J., Brockson, R., De, S., Gray, V., Robinson, D., 2003. Intrinsic dissolution performance testing of the USP dissolution apparatus 2 (rotating paddle) using modified salicylic acid calibrator tablets: proof of principal. Dissolution Technol. 10, 6–15.

McNamara, D.P., Childs, S.L., Giordano, J., Iarriccio, A., Cassidy, J., Shet, M.S., Mannion, R., O'Donnell, E., Park, A., 2006. Use of a glutaric acid cocrystal to improve oral bioavailability of a low solubility API. Pharm. Res. 2, 1888–1897.

Nehm, S.J., Rodríguez-Spong, B., Rodríguez-Hornedo, N., 2006. Phase solubility diagrams of cocrystals are explained by solubility product and solution complexation. Cryst. Growth Des. 6, 592–600.

Nicklasson, M., Brodin, A., Nyqvist, H., 1981. Studies on the relationship between solubility and intrinsic rate of dissolution as a function of pH. Acta Pharm. Suec. 18, 119–128.

O'Connor, K.M., Corrigan, O.I., 2001. Preparation and characterisation of a range of diclofenac salts. Int. J. Pharm. 226, 163–179.

O'Neil, M.J., Heckelman, P.E., Koch, C.B., Roman, K.J. (Eds.), 2006. The Merck Index: An Encyclopedia of Chemicals, Drugs, and Biologicals. , 14th ed. Merck & Co. Inc., Whitehouse Station, NJ, USA.

Padrela, L., Rodrigues, M.A., Velaga, S.P., Matos, H.A., Gomes de Azevedo, E., 2009. Formation of indomethacin–saccharin cocrystals using supercritical fluid technology. Eur. J. Pharm. Sci. 38, 9–17.

Paluch, K.J., Tajber, L., Elcoate, C.J., Corrigan, O.I., Lawrence, S.E., Healy, A.M., 2011. Solid-state characterization of novel active pharmaceutical ingredients: cocrystal of a salbutamol hemiadipate salt with adipic acid (2:1:1) and salbutamol hemisuccinate salt. J. Pharm. Sci., 10.1002/jps.22569.

Rahman, Z., Samy, R., Sayeed, V.A., Khan, M.A., 2011. Physicochemical and mechanical properties of carbamazepine cocrystals with saccharin. Pharm. Dev. Technol., 1–9.

Reddy, L.S., Bethune, S.J., Kampf, J.W., Rodríguez-Hornedo, N., 2009. Cocrystals and salts of gabapentin: pH dependent cocrystal stability and solubility. Cryst. Growth Des. 9, 378–385.

Schultheiss, N., Newman, A., 2009. Pharmaceutical cocrystals and their physicochemical properties. Cryst. Growth Des. 9, 2950–2967.

Stahl, P.H., Wermuth, C.G. (Eds.), 2002. Handbook of Pharmaceutical Salts: Properties, Selection and Use. Wiley-VCH/VHCA, Weinheim/Zürich.

Tajber, L., Corrigan, O.I., Healy, A.M., 2005. Physicochemical evaluation of PVP-thiazide diuretic interactions in co-spray-dried composites—analysis of glass transition composition relationships. Eur. J. Pharm. Sci. 24, 553–563.

Tajber, L., Corrigan, D.O., Corrigan, O.I., Healy, A.M., 2009. Spray drying of budesonide, formoterol fumarate and their composites—I. Physicochemical characterisation. Int. J. Pharm. 367, 79–85.

Trask, A.V., Samuel Motherwell, W.D., Jones, W., 2005. Pharmaceutical cocrystallization: engineering a remedy for caffeine hydration. Cryst. Growth Des. 5, 1013–1021.

Trask, A.V., 2007. An overview of pharmaceutical cocrystals as intellectual property. J. Am. Chem. Soc. 4, 301–309.

Wenger, M., Bernstein, J., 2008. An alternate crystal form of gabapentin: a cocrystal with oxalic acid. Cryst. Growth Des. 8, 1595–1598.

Wermuth, C.G., 2008. The Practice of Medicinal Chemistry, 3rd ed. Elsevier Ltd, p. 750.

Wood, J.H., Syarto, J.E., Letterman, H., 1965. Improved holder for intrinsic dissolution rate studies. J. Pharm. Sci. 54, 1068.

Yu, L.X., Carlin, A.S., Amidon, G.L., Hussain, A.S., 2004. Feasibility studies of utilizing disk intrinsic dissolution rate to classify drugs. Int. J. Pharm. 270, 221–227.